ScienSage

Journal of Advanced Scientific Research

Available online through http://www.sciensage.info

ISSN
0976-9595
Research Article

DNA BINDING, *IN VITRO* CYTOTOXICITY AND ANTICANCER DRUG MECHANISM OF COPPER(II) COMPLEX CONTAINING PYRIDYL-TRIAZINE LIGAND

Jeyaraman Manivel[1], Somasundaram Sangeetha[1,2], Mariappan Murali*[1]

[1]*Coordination and Bioinorganic Chemistry Research Laboratory, Department of Chemistry, National College (Autonomous), Tiruchirappalli, Tamil Nadu, India*

[2]*Department of Chemistry, Tamilavel Umamaheswaranar Karanthai Arts College, Thanjavur, Tamil Nadu, India*

**Corresponding author: murali@nct.ac.in*

ABSTRACT

Mononuclear copper(II) complex $[Cu(dppt)_2(H_2O)_2](ClO_4)_2$ (**1**), where dppt is bidentate $N_{py}N_{tz}$ donor asymmetric ligand (pyridyl-triazine) has been isolated. The X-ray crystal structure of **1** possesses a CuN_4O_2 chromophore with elongated octahedral geometry. The electronic and EPR spectral properties demonstrate that the solvent molecules strongly interacted in the axial position thereby weakens the CuN_4 coordination plane. Absorption and emission spectral and electrochemical measurements clearly show the partial intercalative binding of **1** to calf thymus (CT) DNA. Remarkably, it exhibits potent cytotoxicity (IC_{50}, 3.73 μM) against human cervical carcinoma cells (HeLa), which is 4.5 times better than cisplatin and is non-toxic (IC_{50}, >500 μM) to normal mouse embryonic fibroblasts cells (NIH 3T3). It blocks cell cycle progression of HeLa cells in G1 phase. FACSverse analysis of **1** is suggestive of ROS (reactive oxygen species) generation and absolutely induces apoptotic cell death in HeLa cells.

Keywords: Copper(II) complex, DNA Binding, ROS, Apoptosis, Cytotoxicity.

1. INTRODUCTION

Currently, several reports were highlighting the use of transition metal complexes as anticancer agents [1, 2]. Probably the exception known of those is cisplatin [cis-diamminedichloroplatinum(II)]. It has been extensively used to treat a diffusion of cancers which include testicular, brain, ovarian, bladder, and breast cancer [3]. The scientific success of cisplatin is constrained by its considerable side effects, consisting of nausea, vomiting, and intense nephrotoxicity [3]. Using cisplatin and associated platinum complexes as anticancer agents have inspired a search for other energetic transition metal complexes which can be as powerful, but with lesser side effects. Many biological systems in nature make massive use of metal ions, inclusive of zinc and copper, which play essential roles within the regular functioning of organisms. Transition metals including copper, iron, and manganese, amongst others, are involved in a couple of biological processes from electron transfer to catalysis to structural roles and are often related to active sites of proteins and enzymes [4]. However, dysregulation of some of these vital metals in the course of normal biochemical processing has been implicated in the development of many pathological disorders, together with cancer [5]. These cellular roles simply need the "trace metals" in miniscule however firmly regulated quantities. Through assessment, different metals including arsenic, cadmium, chromium, and nickel are much less useful in view that they produce an extensive variety of toxic facet consequences, which includes carcinogenesis [4,6]. Particularly, copper(II) cation can bind to negatively charged DNA and had been proven to play a crucial function within the nearby formation of hydroxyl radicals [7, 8]. One of the results of excessive copper levels inside the body is a growth within the rate of radical formation mainly to oxidative damage [8]. This results in a disruption of lipid bilayers because of oxidation and cleavage of inclined unsaturated fatty acid residues of phospholipids. Changes in protein features also are promoted via oxidation of thiol and probably amino groups. Gene expression may also be altered because of the oxidation of guanosine and adenosine residues in nucleic acids or altered transcription factor or growth factor activities [9, 10]. More anecdotally, in the human body, Cu binds to N7 of guanine residue of DNA and generates ROS

through the oxidation-reduction reaction resulting in DNA damage and cell apoptosis [11-13]. All these findings aid that the antitumor agent primarily based on Cu could be promising for the treatment of cancer. Therefore, a novel, green coloured copper(II) complex $[Cu(dppt)_2(H_2O)_2](ClO_4)_2$ (**1**), where dppt is 3-(2-pyridyl)-5,6-diphenyl-1,2,4-triazine has been synthesized. Its ability to bind calf thymus (CT) DNA and cancer chemotherapeutic potential against human cervical carcinoma cells (HeLa) and normal mouse embryonic fibroblasts cells (NIH 3T3) has been studied. Also, interesting aspects of the anticancer drug mechanisms underlying the cytotoxic response were probed.

2. EXPERIMENTAL

2.1. Material and methods

Copper(II) acetate monohydrate, 5,6-diphenyl-3-(2-pyridyl)-1,2,4-triazine, $NaClO_4$, *tetra-N*-butylammonium perchlorate (TBAP), ethanol, N,N-dimethyl formamide (DMF), anhydrous ether were of analytical grade and used as received from commercial sources. Calf thymus (CT) DNA was commercially purchased from Sigma Aldrich and stored at -20°C while tris (hydroxymethyl) aminomethane and ethidium bromide (EthBr) were obtained from Merck.

The cell lines HeLa and NIH 3T3 were procured from the NCCS, Pune, India. Cell culture media and reagents were purchased from Hi Media, India. 3-(4,5-Dimethylthiazolyl-2)-2,5-diphenyltetrazolium bromide (MTT) and Annexin V and Apoptosis Detection Kit were purchased from Sigma Aldrich, USA. All antibodies used in this study were procured from Cell Signaling Technology, USA. Ultra-pure Milli-Q water (18.2 μΩ) was used for all experiments.

The elemental analyses (C, H, N) were carried out using a Perkin-Elmer 2400 series II analyzer. The electrical conductivity was obtained with a Systronic 305 conductivity bridge, using 1×10^{-3} M solution of complex in N,N-dimethyl formamide (DMF). FTIR spectra were recorded using a Perkin Elmer Spectrum RX1 FTIR spectrophotometer in the range 400-4000 cm^{-1} with a sample prepared at KBr disc. The electronic spectra were recorded using Perkin Elmer Lambda 365 UV-VIS spectrophotometer using cuvettes of 1 cm length. X-band electron paramagnetic resonance (EPR) measurements were performed at room temperature in the solid state and at 77 K in the DMF solution on JEOL JES-FA200 ESR spectrometer. Emission intensity measurements were carried out using a Shimadzu RF-5301PC spectrofluorophotometer equipped with a thermostatic bath. Solutions of DNA in the 5 mM Tris HCl/50 mM NaCl buffer gave a ratio of UV absorbances at 260 and 280 nm, A_{260}/A_{280}, of 1.9 [14], indicating that the DNA was sufficiently free of protein. Concentrated stock solutions of DNA (13.5 mol dm^3) were prepared in buffer and sonicated for 25 cycles, where each cycle consisted of 30 s with 1 min intervals. The concentration of DNA in nucleotide phosphate (NP) was determined by UV absorbance at 260 nm after 1:100 dilutions. The extinction coefficient, ε_{260}, was taken as 6600 $dm^3\ mol^{-1}cm^{-1}$. Stock solutions were stored at 4°C and used after no more than 4 days. Concentrated stock solutions of copper(II) complex was prepared by dissolving in 2% DMF 5 mM Tris-HCl/50 mM NaCl buffer at pH 7.1 and diluting suitably with the corresponding buffer to required concentrations for all the experiments. For absorption and emission spectral experiments, the DNA solutions were pretreated with solutions of copper(II) complex to ensure no change in concentrations of the copper(II) complex. Cyclic voltammetry (CV) and differential pulse voltammetry (DPV) were performed in a CHI 620C electrochemical analyzer at 25±0.2°C. The working electrode was a glassy carbon disk (0.0707 cm^2) and the reference electrode a saturated calomel electrode. A platinum wire was used as the counter electrode. The supporting electrolyte was *tetra-N*-butylammonium perchlorate (TBAP) or 2% DMF 5 mM Tris-HCl/50 mM NaCl buffer (pH 7.1). Solutions were deoxygenated by purging with nitrogen gas for 15 min prior to measurements; during measurements a stream of N_2 gas was passed over them. The redox potential $E_{1/2}$ was calculated from the anodic (E_{pa}) and cathodic (E_{pc}) peak potentials of CV traces as $(E_{pa} + E_{pc})/2$ and also from the peak potential (E_{pa}) of DPV response as $E_p + \Delta E/2$ (ΔE is the pulse height).

2.2. Synthesis of complex, $[Cu(dppt)_2(H_2O)_2](ClO_4)_2$ (1)

An ethanolic solution (5 mL) of 5,6-diphenyl-3-(2-pyridyl)-1,2,4-trazine (dppt: 0.62 g, 2 mmol) was added dropwise to an aqueous solution (10 mL) of copper(II) acetate monohydrate (0.20 g, 1 mmol). The resulting green coloured solution was stirred for 8 h at room temperature. The product was precipitated as the perchlorate salt by adding stoichiometric equivalent of $NaClO_4$ (0.12 g, 1 mmol) in water (3 mL). The bright

green product,$[Cu(dppt)_2(H_2O)_2](ClO_4)_2$, was collected by suction filtration, washed with cold water and ether and then air-dried. Yield: 76%. Selected IR peaks (ν, cm^{-1}): 3447 b (ν_{O-H}), 1500 m, 1527 s and 1600 w ($\nu_{C=N}$) and ($\nu_{N=N}$), 1103 and 1064 (ν_{ClO4}). Anal. Calcd for $C_{40}H_{32}N_8O_{10}Cl_2Cu$: C, 52.27; H, 3.51; N, 12.19 %. Found: C, 52.32; H, 3.49; N, 12.24 %. Λ_M (DMF): 165 Ω^{-1} cm^2 mol^{-1}. μ_{eff} (27 °C): 1.78 μ_B. Electronic spectrum in DMF [λ_{max}/nm (ε_{max}/dm^3 mol^{-1} cm^{-1})]: 278 (8240), 322 (4885), 494 (35) 688 (30). Electronic spectrum in 2% DMF/5 mM Tris-HCl/50 mM NaCl buffer solution [λ_{max}/nm (ε_{max}/dm^3 mol^{-1} cm^{-1})]: 265 (8350), 292 (4900), 482(45), 676 (40). Room temperature polycrystalline EPR spectrum: g_{iso} = 2.061. EPR spectrum in DMF solution at 77 K: $g_{||}$ = 2.292, $g_\perp$ = 2.060, $A_{||}$ = 165 × 10^{-4} cm^{-1}, $g_{||}/A_{||}$ = 139 cm, G = 4.9. Redox behaviour: $E_{1/2}$ = 0.243 V (CV) and 0.242 V (DPV), ΔE_p= 81 mV, i_{pa}/i_{pc}=1.1, D = 6.2 × 10^6 cm^2s^{-1}.

The blocks of bright green single crystals of $[Cu(dppt)_2(H_2O)_2](ClO_4)_2$ (**1**) separated upon cooling a solution of **1** in MeOH:MeCN:Et_2O at 5 °C for seven days. The latter were found suitable for X-ray studies.

2.3. X-ray crystallography

A bright green needle-like single crystal of the complex $[Cu(dppt)_2(H_2O)_2](ClO_4)_2$ **1** with dimensions 0.35 × 0.30 × 0.30 mm^3 was selected under the polarizing microscope and then mounted on glass fiber. The crystal data collections were performed on a Bruker AXS-KAPPA APEX II diffractometer equipped with a CCD area detector utilizing Mo-K_α radiation (λ = 0.71073 Å) at 273 K. Data were collected and reduced by SMART and SAINT softwares in the Bruker packages [15]. The structure was solved by direct methods and subsequently refined by full-matrix least squares calculations with the SHELXL-2018/3 software package [16]. All non-hydrogen atoms were refined anisotropically while hydrogen atoms were placed in geometrically idealized positions and constrained to ride on their parent atoms. Also, hydrogens on water oxygen which is connected to Cu are located. The disorder in perchlorate anion is fixed and the ratio of occupancies of disordered moieties is found to be 53:47. The graphics interface package used was PLATON, and the figures were generated using the ORTEP 3.07 generation package [17]. Crystallographic data for the structural analysis of $[Cu(dppt)_2(H_2O)_2](ClO_4)_2$ (**1**) have been deposited with Cambridge Crystallographic Data Center, CCDC No. 1994856. Copies of this information may be obtained free of charge from http://www.ccdc.ac.uk /const/ retrieving.html or from the CCDC, 12 Union Road, Cambridge, CB2 1EZ, UK (email: deposit@ccdc. cam.ac.uk).

2.4. Spectroscopic and electrochemical experiments of DNA interactions

The spectroscopic and electrochemical experiments of DNA interactions were carried out by employing the procedure reported by us previously [14].

2.5. Cell viability assays

The in vitro cytotoxicities of test complex **1** (HeLa, 0.1-100 μM; NIH 3T3, 1-500 μM), free dppt ligand, $Cu(OAc)_2{\cdot}H_2O$ against HeLa and NIH 3T3 cell lines were assayed by 3-(4,5-dimethylthiazol-2-yl)-2,5-diphenyltetrazolium bromide (MTT) assay. The inhibitory effect of them on both cancer and normal cells were evaluated by means of their IC_{50} values (concentration of compound required to inhibit 50% of cell proliferation). Cisplatin was chosen as a positive control.

2.6. Anticancer drug mechanistic studies

2.6.1. Cell cycle

The HeLa cells were seeded in 6 well plates with high-glucose DMEM media after the period of the time cells attained the growth and the cells were treated with **1** in its IC_{50} concentration in the medium for 48 h. After 48 h of incubation, cells were trypsinized and resuspended with complete media. Cells were collected and centrifuged at 1000 rpm for 5 min. Then cell pellet was washed with PBS (Phosphate Buffer Saline) twice and subsequently fixed with 1 ml of 70% of ice cold ethanol overnight at 4°C. Following the ice cold ethanol, the cell pellet were washed twice with cold PBS and added 10 μl of RNase A at 10 g/ml concentration, which was then incubated for 30 min and washed with PBS at the end. Cells were then incubated in 1 ml of PBS with 50 μl of propidium iodide (1 mg/ml stock) for 30 min in darkness. Then cells were analysed to check the cell cycle phase using FACSverse flow cytometer (Becton-Dickinson).

2.6.2. ROS generation

The HeLa cells were seeded in 6 well plates with high glucose DMEM media for the treatment until cell

confluency after the cell growth treated with **1** in 3 h, 2 h and 1 h time interval. After the treatment, cells were trypsinized and 10 µM 2',7'-dichlorodihy drofluorescein diacetate (DCHF-DA, Sigma-Aldrich) dye was added to the pellet. This was kept in incubation under darkness for 10 min. The cells were then analyzed to determine ROS level using FACSverse flow cytometer (Becton-Dickinson).

2.6.3. Apoptosis

The HeLa cells were treated with **1** in high-glucose DMEM media for 48 h. After treatment, the cells were trypsinized, resuspended in PBS, washed twice and centrifuged to remove PBS. The cells were suspended in 100 µl of binding buffer containing 5 µl of Annexin V and propidium iodide (PI) and incubated for 15 mins under darkness. Stained cells were diluted using 450 µl of binding buffer. The cells were analyzed by using FACSverse flow cytometer (Becton-Dickinson) and the data were analyzed by FACSverse software.

2.6.4. DAPI staining

Cell nuclear morphology was evaluated by fluorescence microscopy following DAPI (4′,6-diamidino-2-phenylindole) staining. The HeLa cells were treated with **1** for 48 h. The cells were washed with PBS (pH 7.4), fixed with ice cold paraformaldehyde and then cells were then washed with PBS followed by DAPI was added and incubated for 15 min at 37 °C wrapped in aluminium foil. The cells were then washed with PBS and examined under Zeiss Axio Observer fluorescence microscope.

3. RESULTS AND DISCUSSION

3.1. Synthesis and characterization of 1

The bright green complex, $[Cu(dppt)_2(H_2O)_2](ClO_4)_2$ (**1**) was prepared in good yield (76%) and purity by the reaction of an aqueous solution of $Cu(OAc)_2{\cdot}H_2O$, ethanolic solution of 5,6-diphenyl-3-(2-pyridyl)-1,2,4-triazine (dppt) and $NaClO_4$ in a stoichiometric ratio (1:2:1) at room temperature. The selected frequencies observed in the IR spectra of **1**, the broad band appeared at 3447 cm^{-1} represents the existence of H_2O [18]. The stretching vibrations of the C=N and N=N groups appear at considerable lower values with respect to the $\nu_{C=N}$ and $\nu_{N=N}$ of the free dppt ligand supporting the coordination of the pyridyl and triazine nitrogen donors to copper(II) ion [19]. It displays two well split bands at 1103 and 1064 cm^{-1} due to perchlorate anion. Such splitting normally arises due to coordination of or hydrogen bonding [20] of ClO_4^-; however, none of these is present in the crystal structure. Elemental analysis of **1** was entirely consistent with its determined composition by X-ray crystallography. This is substantiated by conductivity measurements in DMF solution, which is expected for a 1:2 electrolyte in solution.

In DMF solution, **1** exhibits only one broad band (λ_{max}, 688 nm) with very low extinction coefficient (ε_{max}, 30 $dm^3\ mol^{-1}\ cm^{-1}$) value in the visible region, typical of ligand field (LF) absorption for Cu(II) located in a tetragonal field. The powder EPR spectrum at 298 K of **1** is isotropic while frozen DMF solution shows axial spectral features, typical of mononuclear Cu(II) species ($g_{||}>g_{\perp}>2.0$; $G = (g_{||}-2)/(g_{\perp}-2) = 4.9$) suggesting the presence of $d_{x^2-y^2}$ ground state in copper(II) located in square-based geometries [21]. The observed $g_{||}$ (2.292) and $A_{||}$ (165×10^{-4} cm^{-1}) values are consistent with the presence of a square based CuN_4 coordination plane with strong axial interaction by two oxygen atoms. The $g_{||}/A_{||}$ quotient (139 cm) is suggestive [22] of negligible distortion from the CuN_4 coordination plane. The electrochemical behaviour of **1** in DMF (TBAP as supporting electrolyte) shows a quasi-reversible redox couple, $E_{1/2}$ at 0.243 V versus SCE. The peak potentials separation, ΔE_p is 81 mV, the ratio of cathodic to anodic peak current (i_{pa}/i_{pc}) is close to unity and the reduction process is diffusion controlled. The weak σ bonding caused by the highly electron-withdrawing phenyl groups as well as strong π back bonding [23] involving the phenyl and pyridine rings, rather than the bulkiness of the ligand molecule, is responsible for the positive $E_{1/2}$ value.

In the complex (**1**), the copper atom is coordinated to two 3-(2-pyridyl)-5,6-diphenyl-1,2,4-triazine (dppt) in *trans* configuration via triazine nitrogen (N_{tz}) and pyridine nitrogen (N_{py}) and two water molecules. The crystallographic data (Table 1) and selected bond lengths and angles (Table 2) are provided.

The two Cu-N_{py} (2.046(2) Å) and Cu-N_{tz} (2.030(2) Å) bond distances are not appreciably different indicating that the donor strength of two nitrogens are equal while the two oxygen atoms of water molecules occupy axial position at longer distances (2.425(3) Å), as a consequence of the Jahn-Teller effect. However, the structure of **1** (Fig. 1) at 273 K is almost the same as that already determined by Palaniandavar et al. [24] at 296 K and Takagi et al. [25] at 200 K and is hence a confirmation of the identity of **1**.

Table 1: Selected crystal data and structure refinement parameters for 1

Formula	$C_{40}H_{32}N_8Cl_2O_{10}Cu$
Formula weight	919.17
Temperature (K)	273(2)
Wavelength (Å)	0.71073
Crystal system	Monoclinic
Space group	*C*2/*c*
a (Å)	12.1016(8)
b (Å)	11.3529(8)
c (Å)	29.8689(18)
α (°)	90
β (°)	92.782(4)
γ (°)	90
V (Å)^3	4098.8(5)
Z	4
D_{calc} (g cm^{-3})	1.490
μ (mm^{-1})	0.732
F(000)	1884
Crystal size (mm)	0.35 × 0.30 × 0.30
θ (°)	2.461-28.159
Reflections collected	21988
Independent reflections	4940
Reflections observed [I > 2σ(I)]	3665
R_{int}	0.0324
GOOF	1.081
R_1 [I > 2σ(I)]	0.0529
wR_2 [I > 2σ(I)]	0.1414
R_1, wR_2 all data	0.0965/0.1567

3.2. Spectroscopic and voltammetric studies on DNA interaction

The absorption spectra of **1** in the absence and presence of DNA at different concentrations (R = [DNA]/[complex] = 1-25) in 2% DMF/5 mM Tris-HCl/50 mM NaCl buffer (pH = 7.1) were recorded (Fig. 2) at 291 nm (π-π^* transition). With an increase in concentration of CT DNA, the hypochromism of 61.0% and red-shift of 3 nm for **1** were observed indicating the partial intercalative interaction. The extent of binding was calculated [26] and the intrinsic equilibrium DNA binding constant, K_b has been estimated to be $2.565\pm0.001\times10^5$ M^{-1}, which suggests the enhanced DNA binding propensity of **1** possibly due to the involvement of partial intercalative interaction of the planar 5,6-diphenyltriazine moiety of coordinated dppt into the DNA base pairs leading to high hypochromism. In addition, there is no change in absorption spectral band of dppt upon increasing the CT DNA concentration indicates that there is no interaction between dppt and the base pairs of DNA.

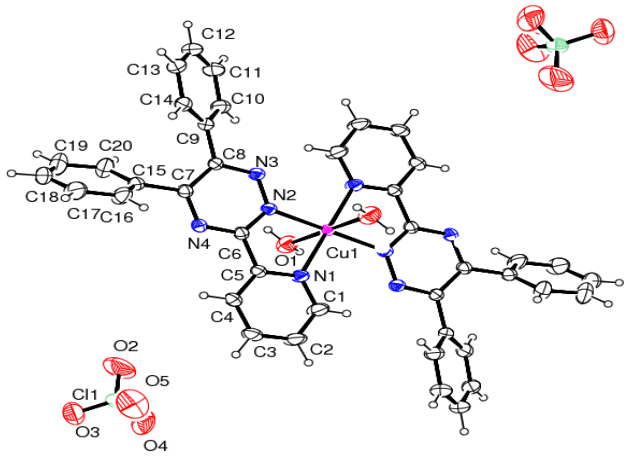

Fig. 1: An ORTEP drawing of $[Cu(dppt)_2(H_2O)_2](ClO_4)_2$ (1) showing 30% probability thermal ellipsoids with atom labeling scheme

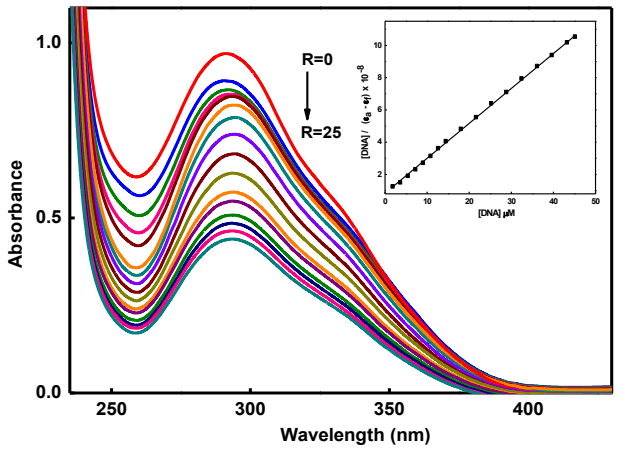

Fig. 2: Absorption spectra of 1 (concentration, 25×10^{-6} M) in 2% DMF/5mM Tris- HCl/50 mM NaCl buffer at pH 7.1 in the absence (R = 0) and presence (R = 25) of increasing amounts of CT DNA. Inset: Plot of [DNA] vs [DNA]/(ε_a - ε_f) at R = 25 of 1.

The intrinsic fluorescence intensity of DNA and that of EthBr are low, while the fluorescence intensity of EthBr will be enhanced on addition of DNA due to its intercalation into the DNA. In our experiment, the fluorescence intensities of EthBr-DNA system show a decreasing trend with increasing concentration of **1** (Fig. 3), indicating that some EthBr molecules are

released from EthBr-DNA after an exchange with **1** which results in the fluorescence quenching of EthBr. This may be due to that **1** displaces the EthBr from its DNA-binding sites in the competitive manner. The plot (Fig. 3, inset) illustrates that the quenching of EthBr bound to DNA are in good agreement with the linear Stern-Volmer equation [27]. The K_{SV} value (1.60×10^5 M^{-1}) of **1** indicates the quenching efficiency and especially significant degree of binding to DNA. The binding strength of **1** (only those samples caused a 50% decrease of fluorescence intensity) with DNA was estimated as apparent binding constant (K_{app}) [28].

Table 2: Selected bond lengths (Å) and bond angles (°) for 1

N(2)-Cu(1)	2.030(2)	N(2)-Cu(1)#1	2.030(2)
N(1)-Cu(1)	2.046(2)	N(1)-Cu(1)#1	2.046(2)
O(1)-Cu(1)	2.425(3)	O(1)-Cu(1)#1	2.425(3)
N(2)-Cu(1)-N(2)#1	180.0 (9)	N(2)-Cu(1)-N(1)#1	100.14(9)
N(2)#1-Cu(1)-N(1)#1	79.86(9)	N(2)-Cu(1)-N(1)	79.86(9)
N(2)#1-Cu(1)-N(1)	100.14(9)	N(1)#1-Cu(1)-N(1)	180.0 (9)
N(2)-Cu(1)-O(1)#1	90.39(10)	N(2)#1-Cu(1)-O(1)#1	89.61(10)
N(1)#1-Cu(1)-O(1)#1	88.83(11)	N(1)-Cu(1)-O(1)#1	91.17(11)
N(2)-Cu(1)-O(1)	89.61(10)	N(2)#1-Cu(1)-O(1)	90.40(10)
N(1)#1-Cu(1)-O(1)	91.17(11)	N(1)-Cu(1)-O(1)	88.83(11)
O(1)#1-Cu(1)-O(1)	180.0 (9)		

Symmetry transformations used to generate equivalent atoms: #1 -x+1/2,-y+1/2,-z+1

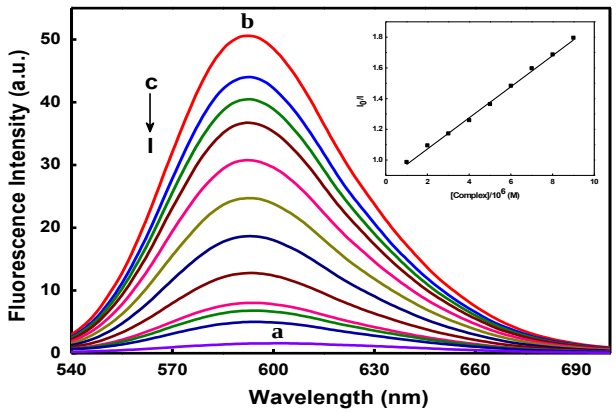

Inset: Plot of [complex × 10^{-6}] vs I_0/I of 1.

Fig. 3: Fluorescence quenching curves of ethidium bromide bound to DNA in 2% DMF/ 5mM Tris-HCl/50 mM NaCl buffer at pH 7.1: (a) EthBr (1.25 µM); (b) EthBr + DNA (125 µM); (c-m) EthBr + DNA + 1 (0-9 µM).

The K_{app} value (2.82×10^5 M^{-1}) supports a strong interaction of **1** with CT DNA and the mode of binding through partial intercalation [29]. The results are consistent with those obtained from electronic absorption titration studies. The cathodic (0.032 V) and anodic peak potential (0.132 V) values observed from the cyclic voltammetric (CV) responses for **1** in 2% DMF-5 mM Tris-HCl-50 mM NaCl buffer (pH = 7.1), which correspond to Cu^{II}/Cu^{I} redox couple [30]. Upon addition of DNA, both the cathodic and anodic current decreases drastically (Fig. 4), this is expected of strong binding of the complex with DNA [31] via partial intercalation. The formal potentials of Cu^{II}/Cu^{I} couple (obtained from differential pulse voltammetry (DPV) s tudies) in the E^0f (0.116 V) and E^0b (0.032 V) forms shift negatively (-84 mV) after reacting with DNA. The ratio of equilibrium binding constants, K_+/K_{2+}, is calculated to be 0.04, which suggests that the B form of DNA tends to stabilize Cu(II) over Cu(I) state.

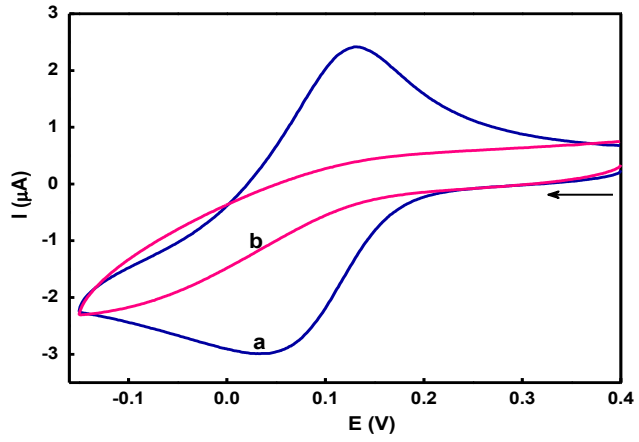

Fig. 4: Cyclic voltammograms of 1 (0.5 mM) in the absence (a) and presence (b) of CT DNA (R = 5) at 25.0 ± 0.2 °C at 50 mV s^{-1} scan rate in 2% DMF/5mM Tris-HCl/50 mM NaCl buffer at pH 7.1.

3.3. *In vitro* cytotoxic activity

HeLa cells were treated with increasing concentrations (0.1 to 100 μM) of **1** for 48 h inhibited the growth of HeLa cells in a dose-dependent manner (IC_{50}, 3.73 ± 0.57 μM) (Fig. 5).

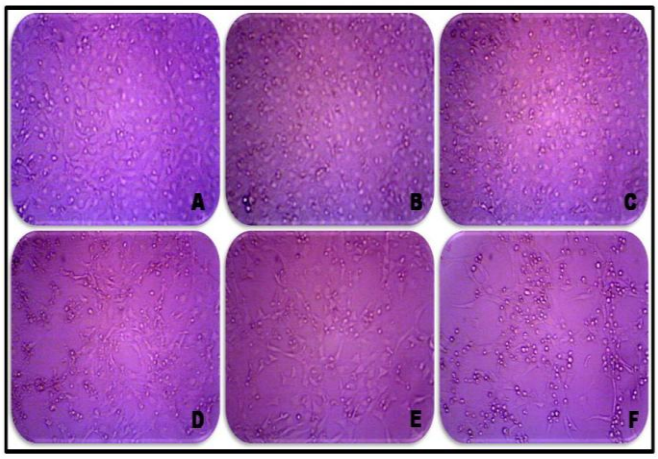

Fig. 5: Photomicrograph of human cervical carcinoma cells (HeLa) after 48 h exposure with 1 (A, control; B, 0.1 μM; C, 1 μM; D, 10 μM; E, 50 μM; F, 100 μM).

From the IC_{50} of **1**, we can find that it is found to be highly active against the selected cancer cells [32] and 4.5 times better than cisplatin (IC_{50}, 16.4 μM). In comparison, free dppt ligand (IC_{50}, 112.48 μM) and $Cu(OAc)_2 \cdot H_2O$ (IC_{50}, 705.67 μM) showed no significant growth inhibition activities, which indicated that the chelation of dppt with copper ion was essential for anticancer activities of the copper(II) complex. In addition, the results indicated that the IC_{50} value of **1** against NIH 3T3 mouse embryonic fibroblasts (normal cells) is found to be above 500 μM, which confirmed that **1** is very specific on cancer cells. Finally, the cytotoxic behaviour of **1** is consistent with its ability to bind with DNA.

3.4. Anticancer drug mechanism

The profiles of propidium iodide stained HeLa cells treated with IC_{50} concentration of **1** for 48 h were analyzed by FACS [33]. As shown in Fig. 6, in the control, the percentage in the cell at G1 phase is 61.94% and the remarkable increase of 17.2% was found. The increase in G1 phase was accompanied by the corresponding reduction in G0, S and G2/M phases. The data mean that **1** induces cell cycle arrest at G1 phase in HeLa cells. The cells treated with **1** and DCFDA for 1 h show significant shift of the histogram towards the right, indicating an increase in the intensity of emission resulting from the generation of DCF from DCFDA [34]. As shown in Fig. 7, in the control, the DCF fluorescence intensity is 100% while the intensity of DCF fluorescence increases to 128% when HeLa cells were incubated with **1**.

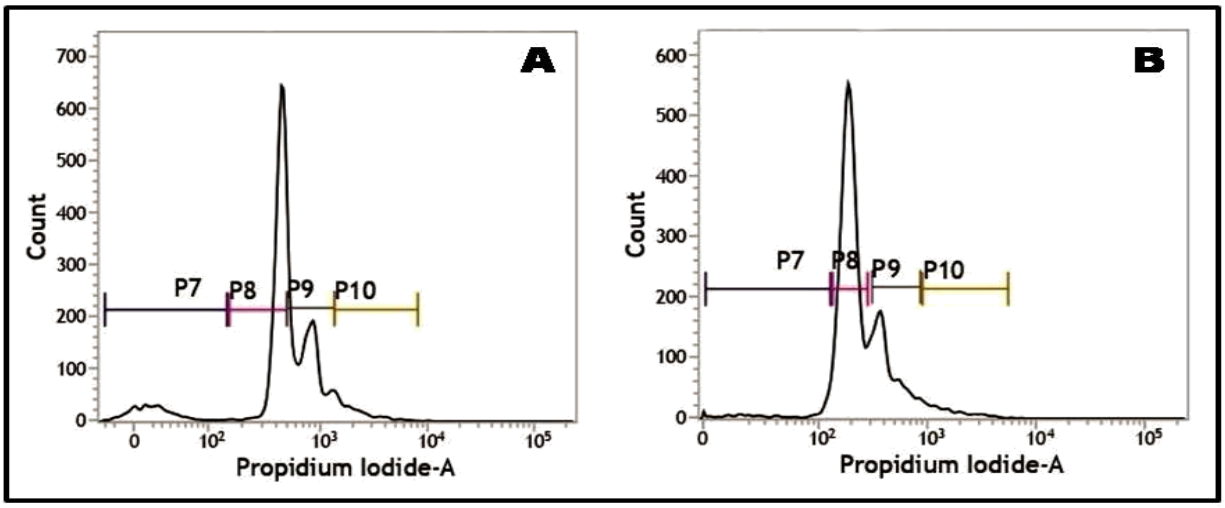

Fig. 6: Flow cytometric analysis showing the G1 phase cell cycle arrest by 1 in HeLa cells (P7, P8, P9 and P10 correspond to G0, G1, S and G2/M phases respectively). A, HeLa cells alone; B, HeLa cells treated with 1.

Greater shift implies higher fluorescence intensity resulting from higher amount of DCF formation and thus greater ROS generation, which is consistent with the apoptotic effect (cf. below) of **1**. Moreover, the ROS levels induced by **1** show a time-dependent manner, decreasing the fluorescence intensity for 2 h (119%) and 3 h (116%). The result demonstrates the generation of ROS and this reactive species possibly causing cell apoptosis. We then carried out apoptosis assay to further evaluate the possible mechanism of cell death induced by **1** [35]. In the control cells, the percentage of living, early apoptotic, late apoptotic and necrosis cells were 99.9, 0.0, 0.1 and 0.0%, respectively (Fig. 8).

However, **1** treated HeLa cells displayed a remarkable average of 56.08% of early apoptotic cells and 18.33% of late apoptotic cells. The increased expression of Annexin V positive cells undoubtedly demonstrated the cells were in apoptosis stage and is consistent with its *in vitro* cell cytotoxicity. Interestingly, there is no sign of cell death via necrotic pathway. To understand the nuclear morphology and the nature of cell death mechanism, we have carried out DAPI (4′,6-diamidino-2-phenylindole) staining with **1** (Fig. 9).

The control HeLa cells exhibited evenly stained nucleus with round and intact contours whereas the treated cells showed characteristic fragmentation of the nucleus or condensed nuclei which is supportive of the cell toxicity induced by **1** due to apoptotic mode of cell death.

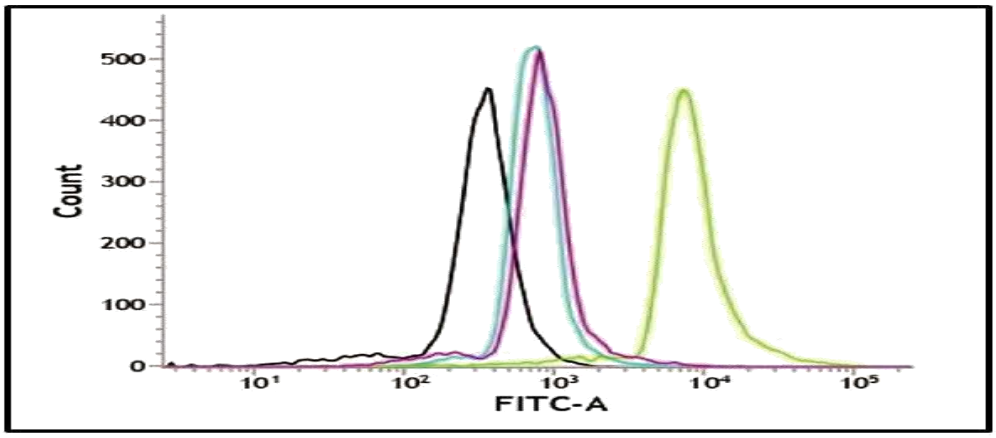

Fig. 7: DCFDA assay in HeLa cells for generation of ROS using the 1 in a time-dependent manner (control, black; 1 h, blue; 2 h, red; 3 h, green).

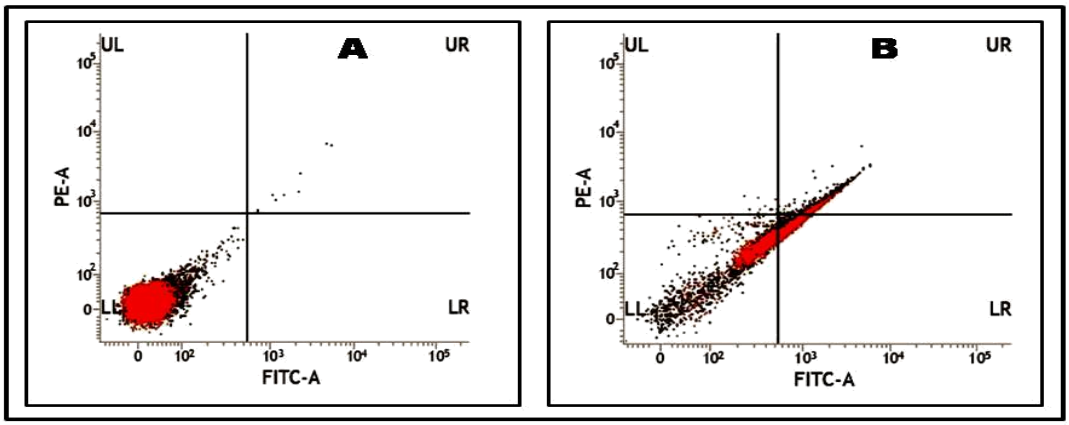

Fig. 8: Cellular apoptosis induced by 1 as determined from the annexin V-FITC/PI staining assay of the HeLa cells with four distinct phenotypes: viable cells (lower left quadrant, LL); cells at an early stage of apoptosis (lower right quadrant, LR); cells at a late stage of apoptosis (upper right quadrant, UR); and necrosis (upper left quadrant, UL). A, HeLa cells alone; B, HeLa cells treated with 1; red dots, gated cells; black dots, ungated cells.

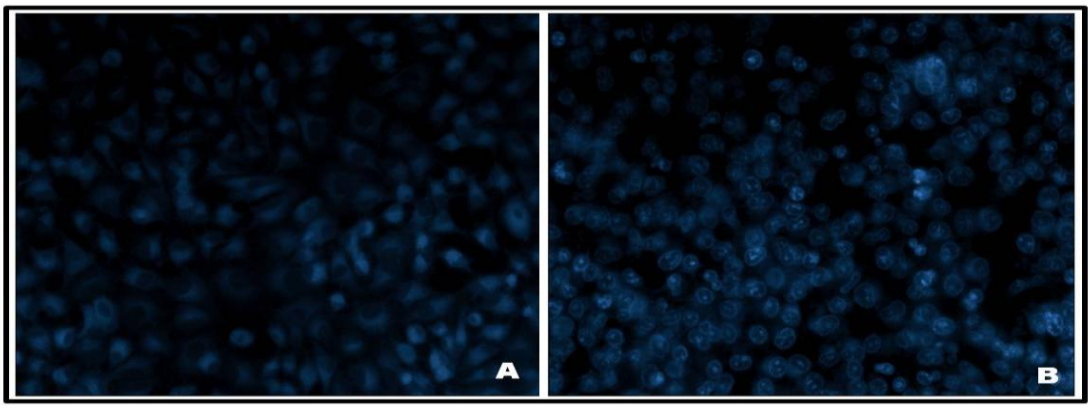

Fig. 9: HeLa cells stained with DAPI (A, HeLa cells alone; B, HeLa cells treated with 1) and visualized under a fluorescence microscope.

4. CONCLUSION

The copper(II) complex, $[Cu(dppt)_2(H_2O)_2](ClO_4)_2$, has been synthesized and characterized. The complex binds to CT DNA through partial intercalative mode. It exhibits highly active inhibitory effect, which was higher than cisplatin and selective to cancer cells while non-toxic to healthy cells. The biological evaluation provides evidence that it blocked cell cycle at G1 phase and induced apoptosis alone along with the generation of ROS. The present lead complex is a novel therapeutic agent for the treatment of cervical cancer as well as encourages further exploration of non-platinum anticancer agents. It targets the mitochondria of cancer cells and induces apoptosis by a mechanism involving the formation of ROS.

5. ACKNOWLEDGEMENTS

We are grateful to the DST-FIST programme of the National College (Autonomous), Tiruchirappalli. Thanks are due to STIC, Cochin University of Science and Technology for X-ray crystal structure data. We thank SAIF, Indian Institute of Technology Madras for structure solution and refinement (Dr. P. K. Sudhadevi) and for recording EPR spectra.

6. REFERENCES

1. Ndagi U, Mhlongo N, Soliman ME. *Drug Des Dev Ther*, 2017; **11**:599-616.
2. Frezza M, Hindo S, Chen D, Davenport A, Schmitt S, Tomco D, Dou QP. *Curr Pharm Des*, 2010; **16**:1813-1825.
3. Marzano C, Trevisan A, Giovagnini L, Fregonal D. *Toxicol In Vitro,* 2002; **16**:413-419.
4. Orvig C, Abrams MJ. *Chem Rev,* 1996; **99**:2201-2204.
5. Yaman M, Kaya G, Yekeler H. *World J Gastroenterol* 2007; **13**:612-618.
6. Thompson KH, Orvig C. *Science* 2003; **300**:936-939.
7. Samuni A, Chevion M, Czapski G. *J Biol Chem*, 1981; **256**:12632-12635.
8. Wijker CA, Lafleur MV. *Mut Res*, 1999; **429**:27-35.
9. Linder MC. *Mut Res*, 2001; **475**:141-152.
10. Deegan C, Coyle B, McCann M, Devereux M, Egan DA. *Chem-Biol Interact,* 2006; **164**:115-125.
11. Knox JJ, Hotte SJ, Kollmannsberger C, Winquist E, Fisher B, Eisenhauer EA. *Invest New Drugs,* 2007; **25**:471-477.
12. Yuan J, Lovejoy DB, Richardson DR. *Blood*, 2004; **104**:1450-1458.
13. Barnham KJ, Masters CL, Bush AI. *Nat Rev Drug Discov*, 2004; **3**:205-214.
14. Sangeetha S, Murali M. *Int J Biol Macromol*, 2018; **107**:2501-2511.
15. Bruker AXS. Inc SMART (Version 5.060) and SAINT (Version 6.02), Madison, Wisconsin: USA; 1996.
16. Sheldrick GM. *Acta Cryst*, 2015; **C17**:3-8.
17. Farrugia LJ. *J Appl Cryst*., 2012; **45**:849-854.
18. Nakamoto K. Infrared and Raman spectra of inorganic and coordination compounds. 4th edn. Wiley- Interscience, New York; 1986.
19. Bereau V, Marrot J.*CR Chim*, 2005; **8**:1087-1092.
20. Rosenthal MR. *J Chem Educ*, 1973; **50**:331-335.
21. Moradi-Shoeili Z, Amini Z, Boghaei DM, Notash B. *Polyhedron*, 2013; **53**:76-82.
22. Loganathan R, Ramakrishnan S, Suresh E, Riyasdeen A, Akbarsha MA, Palaniandavar M. *Inorg. Chem,* 2012; **51**:5512-5532.

23. Lever ABP. Inorganic Electronic Spectroscopy. Elsevier: Amsterdam; 1984.
24. Uma R, Palaniandavar M, Butcher RJ. *J Chem Soc Dalton Trans*, 1996; 2061-2066.
25. Yamada A, Mabe T, Yamane R, Noda K, Wasada Y, Inamo M, et al. Dalton Trans, 2015; **44**:13979-13990.
26. Wolfe A, Shimer Jr. GH, Meehan T. *Biochemistry*, 1987; **26**:6392-6396.
27. Lakowicz JR, Webber G. *Biochemistry*, 1973; **12**:4161-4170.
28. Lee M, Rhodes AL, Wyatt MD, Forrow S, Hartley JA. *Biochemistry*, 1993; **32**:4237- 4245.
29. Kahrovic E, Zahirovic A, Turkusic E. *J Chem Chem Eng*, 2014; **8**:335-343.
30. Monica B, Marisa BF, Franco B, Giorgio P, Silvana P, Pieralberto T. *Inorg Chem*, 2003; **42**:2049-2055.
31. Bard AJ, Faulkner LR. Electrochemical Methods: Fundamentals and Applications. Wiley: New York; 1980.
32. Tarafder MTH, Kasbollah A, Crouse KA, Ali AM, Yamin BM, Fun HK. *Polyhedron*, 2001; **20**:2363-2370.
33. Crowley LC, Marfell BJ, Scott AP, Waterhouse NJ. *Cold Spring Harb Protoc*, 2016; **11**:953-956.
34. Takanashi T, Ogura Y, Taguchi H, Hashizoe M, Honda Y. *Investig Ophthalmol Vis Sci*, 1997; **38**:2721-2728.
35. Bhattacharjee RN, Park KS, Kumagai Y, Okada K, Yamamoto M, Uematsu S, et al. *J Biol Chem*, 2006; **281**:36897-36904.